Electronic Supplementary Material (ESI) for Lab on a Chip.
This journal is © The Royal Society of Chemistry 2014

Novel side electrode configuration integrated in fused silica microsystems for synchronous optical and electrical spectroscopy

Sertan Sukas, Erik Schreuder, Bjorn de Wagenaar, Joost Swennenhuis, Albert van den Berg, Leon Terstappen, and Séverine Le Gac

ELECTRONIC SUPPLEMENTARY INFORMATION

1. Details of fabrication process flow:

First, 500 µm thick, 100 mm diameter, high quality surface finish fused silica wafers (Mark Optics, Santa Ana, USA) were cleaned in liquid and fuming nitric acid solutions. Then each wafer in the stack was processed separately (same process steps, e.g. cleaning, etching were performed in the same batch) before bonding.

The following steps were performed for wafer A: 1. Spin-coating of photoresist (PR) at 4000 rpm for 1 µm thickness. 2. Patterning of PR (electrode layout) via ultraviolet (UV) photolithography. 3. Baking of photoresist at 120 °C for 10 min for solvent removal before immersion into the liquid. 4. Wet chemical etching in buffered hydrogen fluoride solution (BHF) for 300 nm depth. 5. Sputtering Tantalum-Platinum (Ta-Pt) metal layers for a total thickness of 300 nm. 6. Ultrasonic bath treatment in Acetone and Isopropanol (IPA), respectively for lift off process for obtaining recessed electrodes. 7. Spin-coating of PR at 1000 rpm for 10 µm thickness. 8. Patterning of PR (channel layout) via UV photolithography. 9. Baking of photoresist at 150 °C for 2 h for solvent removal. 10. Deep reactive ion etching (DRIE) for the half depth of the channel. 11. PR removal in oxygen plasma for 30 min followed by piranha cleaning for 10 min.

The following steps were performed for wafer B: 1. Spin-coating of PR at 1000 rpm for 10 µm thickness. 2. Patterning of PR (mirrored channel layout) via UV photolithography. 3. Baking of photoresist at 150 °C for 2 h for solvent removal. 4. Deep reactive ion etching (DRIE) for the half depth of the channel. 5. Laminating the thick photosensitive foil on the back side of the wafer. 6. Patterning of the photosensitive foil (reservoir opening layout). 7. Powder blasting of the wafer for opening through holes for fluidic connections. 8. Ultrasonic bath treatment in Acetone and Isopropanol (IPA), respectively for removal of the foil. 9. PR removal in oxygen plasma for 30 min followed by piranha cleaning for 30 min. 10. Deposition of BPSG layer for 300 nm thickness via plasma enhanced chemical vapor deposition (PECVD). 11. Annealing at 900 °C for 2 h for the reflow of the BPSG layer.

As a next step, the pre-bond (direct bonding) was obtained for wafers A and B after the alignment and subsequently the stack was placed into the oven at 900 °C for 3 h for creating the permanent bond. Finally, the stack was diced into the individual microchips.

Note on the electrode thickness: Although there is no limitation on the electrode thickness arising from the fabrication techniques, there are practical limits that we have set in this study. The realization of the recessed electrodes consists of two steps as described above: wet etching and sputtering. Both techniques have no limits on etch depth or film thickness, therefore fabricating electrodes with a thickness from a few nanometers to tens of micrometers is possible. However, the required electrode thickness for creating a uniform and homogeneous electric field distribution with a sufficient intensity over the entire cross section of the microchannel is related to the channel depth. Since we set a fixed depth of 40 µm to cover the whole range of cells that we study without clogging, 300 nm electrode thickness was sufficient to obtain the desired electric field distribution. In addition, the process limitation for sputtering in MESA+ Nanolab facilities for the maximum thickness of Pt or Gold (Au) targets is 500 nm due to the material and equipment costs.

2. Simulation of electric field distribution inside the microchannels:

Multiphysics simulations were performed using COMSOL 4.3a to determine the electric field distribution inside the channels when the proposed side electrode configuration is used. As a model geometry, a 20 µm wide, 40 µm deep microchannel equipped with 30 nm thick metal electrodes was used. The electrical properties of the flow medium was defined as same as 1X PBS solution. Fig. ESI 1 shows the electric field distribution as well as the

potential drop over the cross section of the channel for the application of a DC potential of 16 V. Although AC potentials were applied during the lysis experiments, the created electric field over the cell membrane was not different than a DC application since the charging times of the cell membrane were significantly smaller than the period of the applied potentials. Fig. ESI 2 represents the electric field change at the center line of the cross section of the channel.

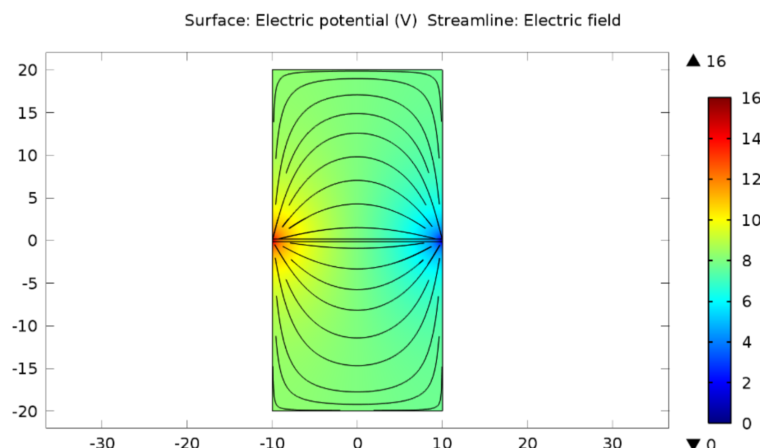

Fig. ESI 1 Electric field distribution inside the microchanel equipped with side electrodes. Stream lines represent the electric field, while surface plot represents the potential distribution. Uniform electric field distribution is obtained.

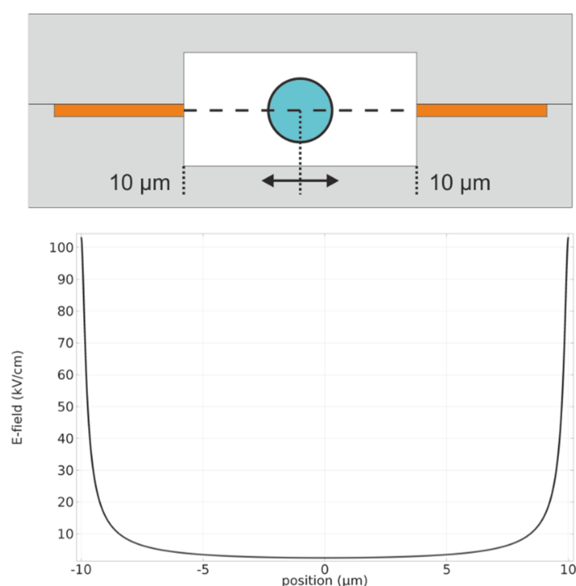

Fig. ESI 2 Electric field change over the center line of the cross section of the microchannel.

3. Experimental data of a continuous electrical lysis experiment

As mentioned in the main text, the microchips were designed for continuous flow electrical lysis experiments. To evaluate the performance of the electrode configuration, cells were also lysed in continuous flow mode using a narrow constriction of 10 µm width. Fig. ESI 3 shows the variations in fluorescence intensity inside the cells as a function of time for 5 subsequent lysis events. Signal amplitudes are normalized taking the minimum signal level obtained after the lysis is completed as a reference to clearly show the trend and the amount of the decrease in the signals. Experiments were performed using the same sample and buffer compositions as described in the main text. This set of experiments was performed with a continuous flow generated at 50 mbar pressure and the applied voltage was 10 V_{PP} at 20 kHz.

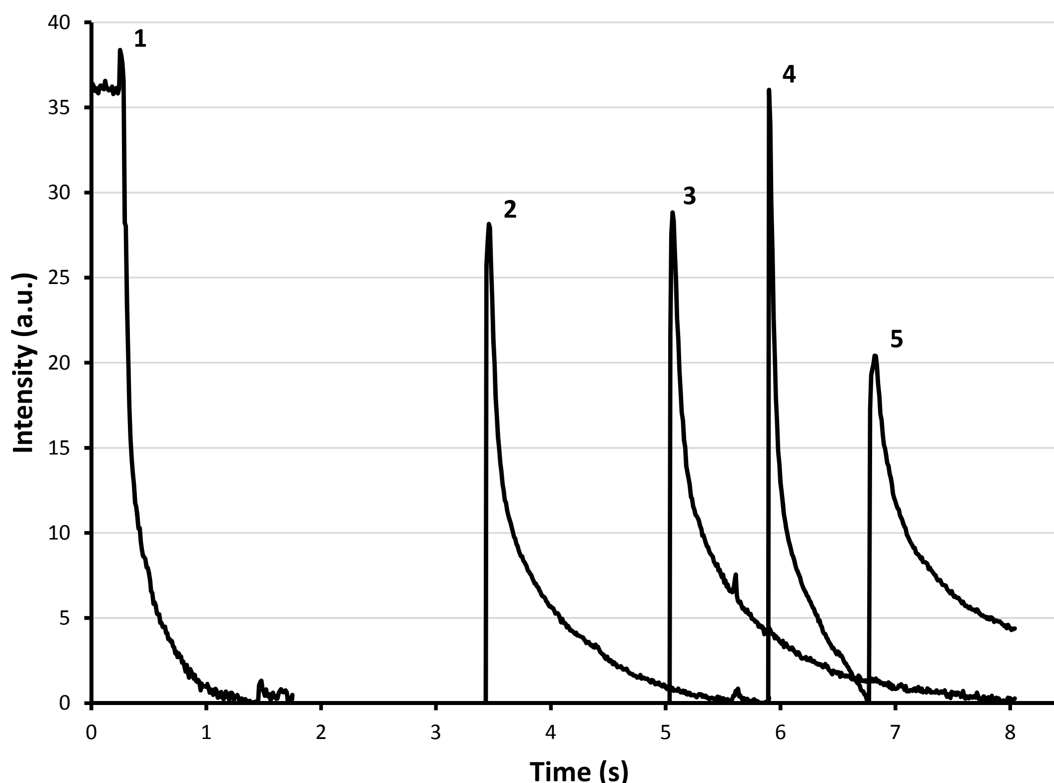

Fig. ESI 3 Variations in fluorescence intensity inside the cells as a function of time for 5 subsequent and individual electrical lysis events in 8 s. in continuous flow mode in a 10 µm wide constriction. Data are normalized taking the minimum signal level obtained after the lysis as a reference. Higher initial signal amplitude corresponds to a larger cell size. The similar decay trends in signal amplitude shows the stability of the system and the repeatability of the experiments.

4. Experimental data of the electrical impedance measurements

Impedance changes upon cell passing were measured using an Andeen Hagerling 2700A capacitance bridge connected to the side electrode pairs. The in-phase (dielectric loss) and out-phase (capacitance) components of the impedance, directly reported by the capacitance bridge, were used to derive the total impedance using custom MATLAB (R2010b) script. The impedance baseline, composed of the impedance of the electric double layer, electrolyte resistance and stray resistance, is detected and corrected for by the script, allowing automated peak detection of cell passing events. Fig. ESI 3 represents the graphs generated during the frequency sweep for 1X PBS solution without any cells. Fig. ESI 4, 5 and 6 represent the capacitance, loss and corresponding impedance change versus elapsed time for the measurements mentioned in the paper. Generated impedance data were plotted together with the synchronized optical measurements (Fig. ESI 7). The movie recorded via fluorescence imaging was decomposed into individual frames and profile plots matched with the time data were generated using an image analyses software. The same detection window was defined for optical data analysis as electrical impedance measurements as mentioned in the main text.

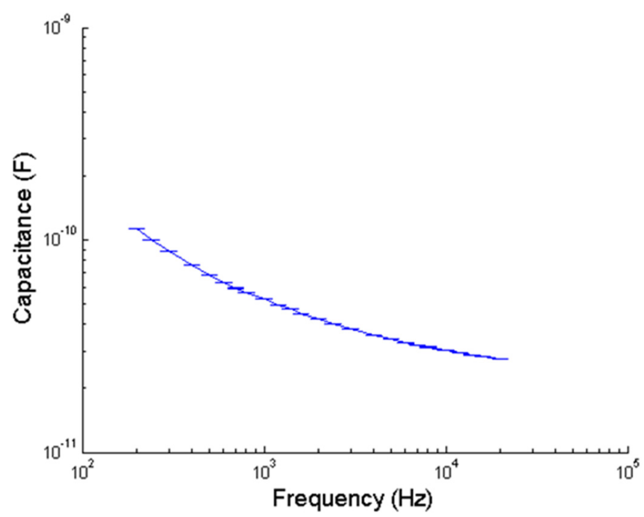

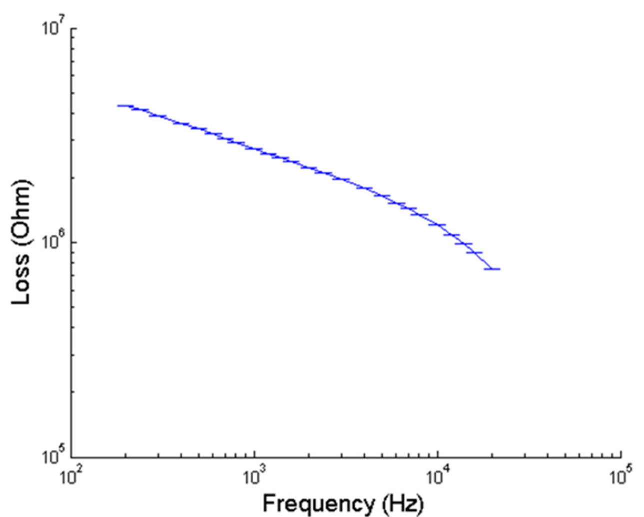

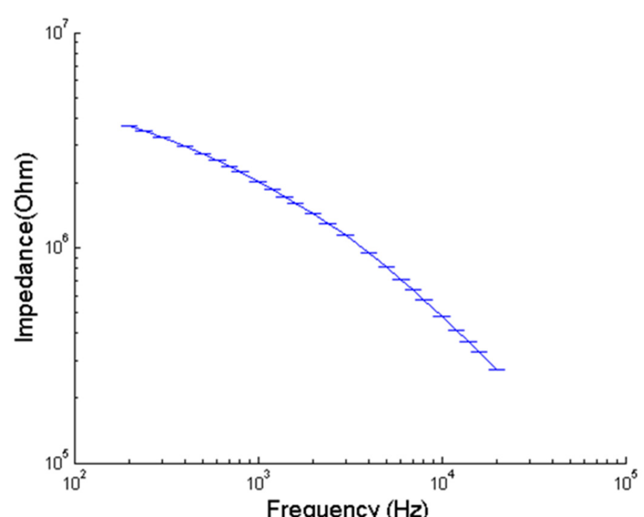

Fig. ESI 4 Capacitance, loss and impedance sweep.

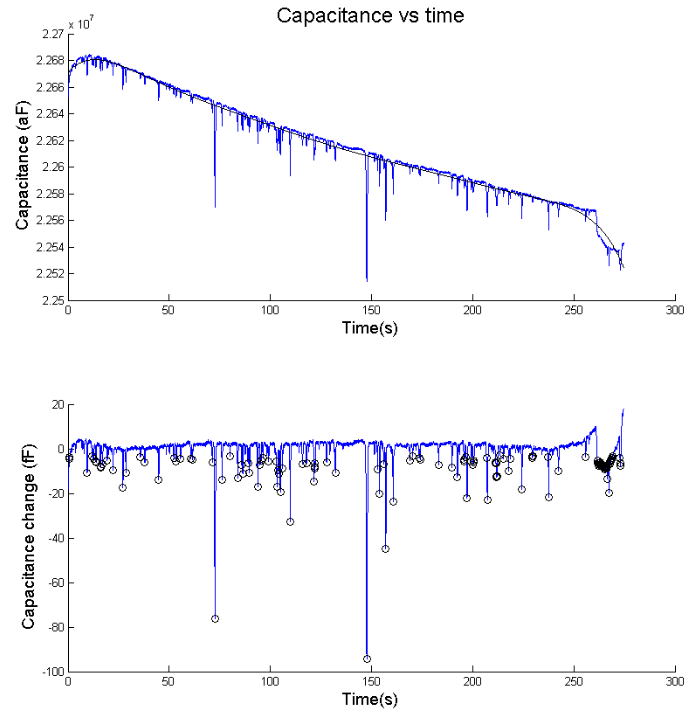

Fig. ESI 5 Baseline fitted data (top) and filtered data with peak detection (bottom) for capacitance change.

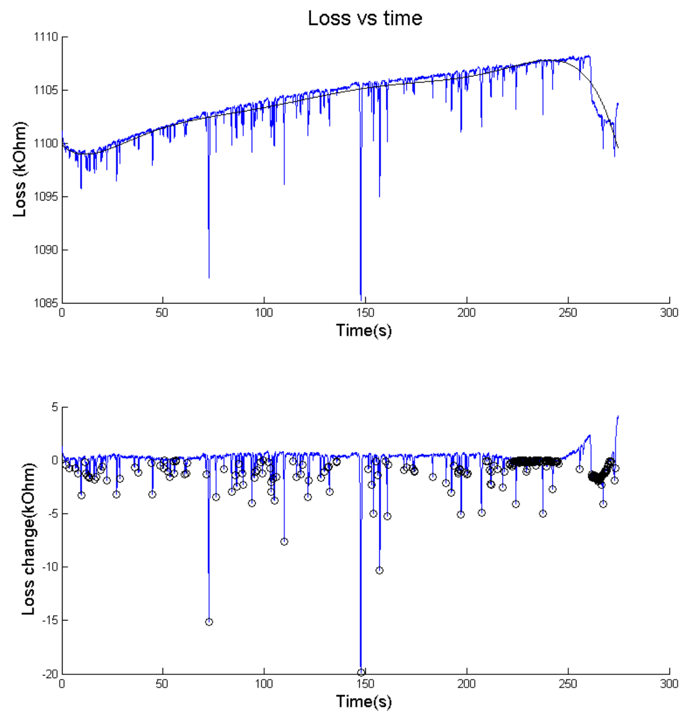

Fig. ESI 6 Baseline fitted data (top) and filtered data with peak detection (bottom) for loss change.

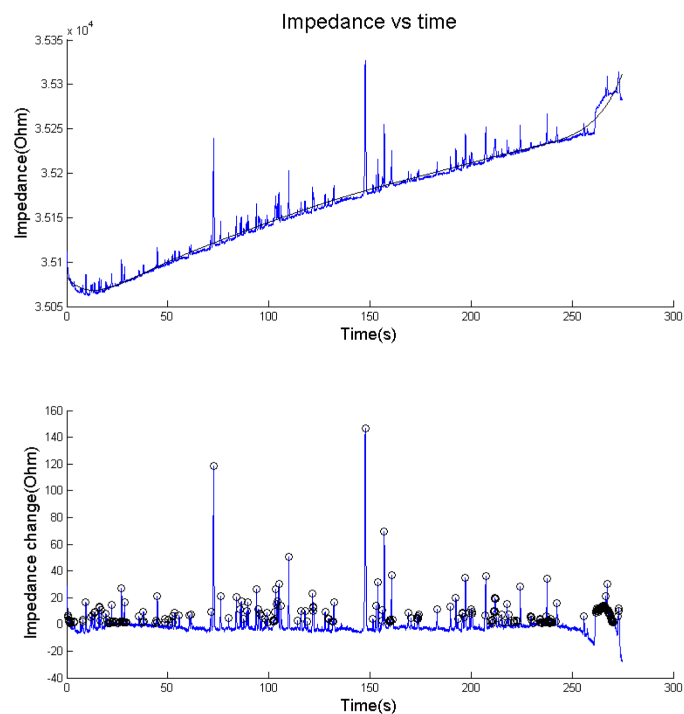

Fig. ESI 7 Baseline fitted data (top) and filtered data with peak detection (bottom) for impedance change.

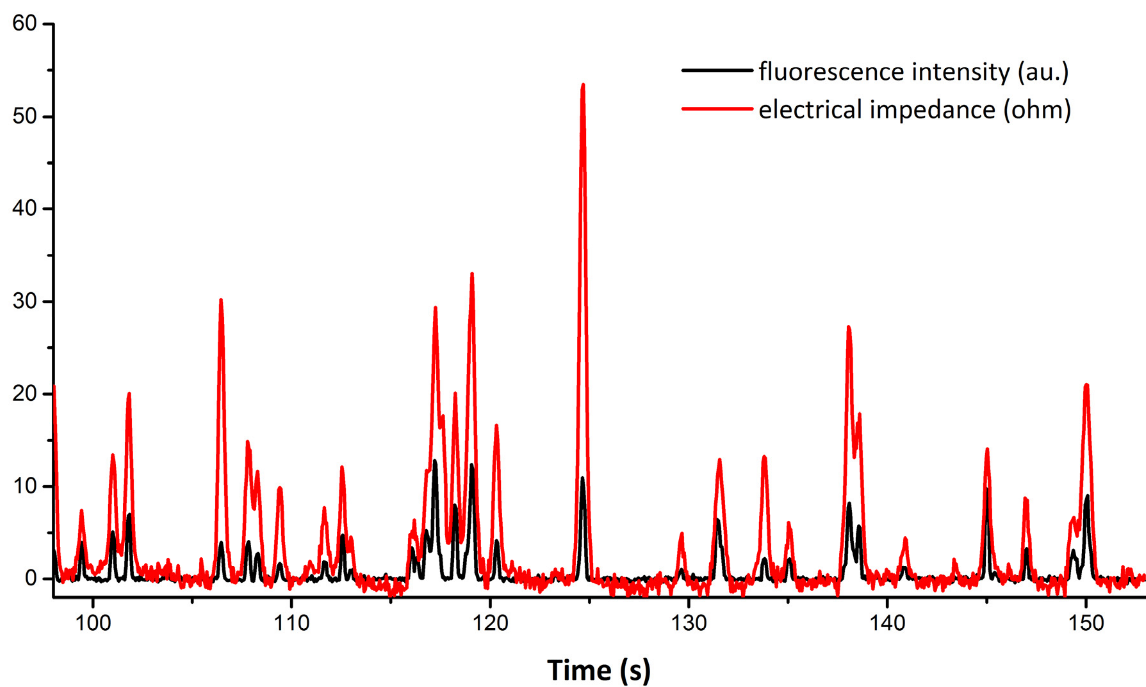

Fig. ESI 8 Data obtained from synchronous optical and electrical measurements of cells. Data sets fit perfectly. Please note that only a portion of the entire data (50 s duration) is illustrated for the sake of clarity.

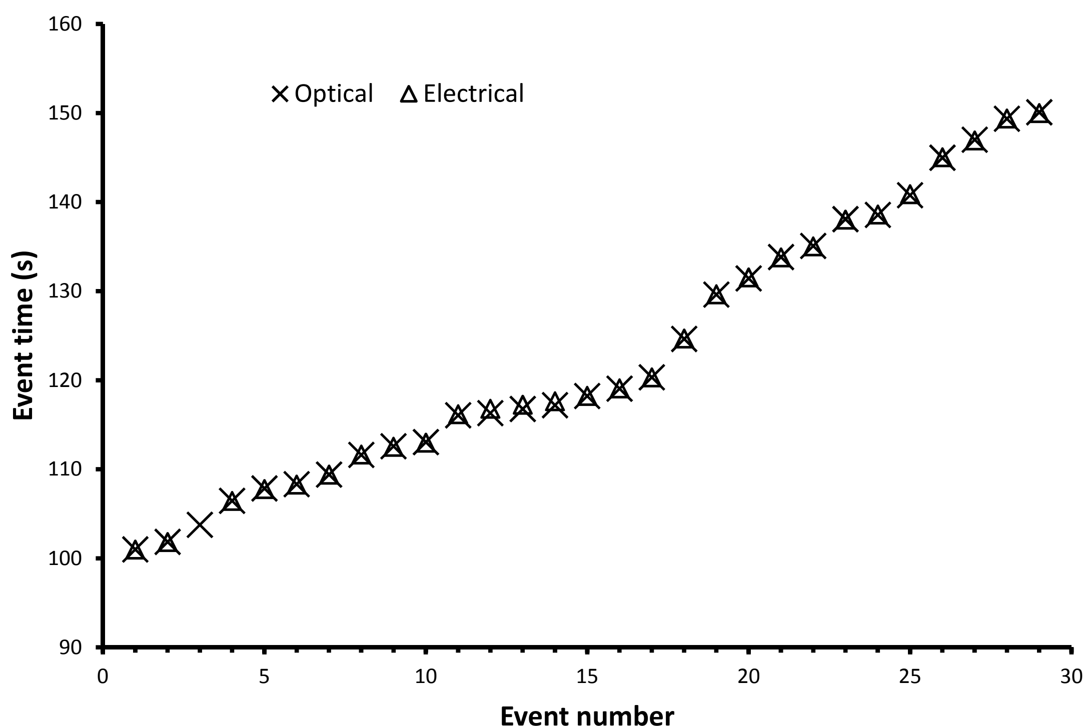

Fig. ESI 9 Detected (cell passing) events (x-axis) and their corresponding times (y-axis) for the same time period as shown in Fig. ESI 8. 29 events were detected via optical measurements, while electrical impedance resulted in 28 events. The 3rd optical event of was a false positive (there was no cell but a fluorescent dust). Both data sets fit perfectly, as the detected peak centers (time axis on Fig. ESI 8) show a perfect match.

Table ESI 1 Detected (cell passing) events and their corresponding times (peak centers on the time axis) for the same time period as shown in Fig. ESI 9. 29 events were detected via optical measurements, while electrical impedance resulted in 28 events. The 3rd optical event of was a false positive. The maximum difference between the signals is less than 50 ms.

Event #	Optical (s)	Electrical (s)	Difference (ms)
1	101.00	100.99	1.32
2	101.84	101.82	1.66
3	103.76	No peak	
4	106.46	106.45	1.11
5	107.84	107.79	5.29
6	108.32	108.29	2.77
7	109.40	109.41	0.81
8	111.62	111.65	2.42
9	112.58	112.54	4.48
10	113.06	112.98	7.98
11	116.06	116.18	12.12
12	116.30	116.79	49.18
13	116.78	117.24	46.36
14	117.20	117.64	43.41

15	118.22	118.25	2.82
16	119.06	119.09	2.47
17	120.32	120.32	0.48
18	124.64	124.68	3.73
19	129.62	129.66	3.70
20	131.42	131.55	13.37
21	133.82	133.79	3.02
22	135.08	135.03	5.41
23	138.08	138.04	3.70
24	138.56	138.61	4.60
25	140.78	140.89	11.33
26	144.98	145.03	4.95
27	147.02	146.94	8.47
28	149.36	149.39	2.83
29	150.08	150.01	7.31